Materials Advances

ROYAL SOCIETY OF CHEMISTRY

PAPER

View Article Online
View Journal | View Issue



Cite this: *Mater. Adv.*, 2024, 5, 1137

# Lipid nanoparticles as efficient verteporfin nanocarriers for photodynamic therapy of cancer†

Tomás Mendes, Andreia Granja * and Salette Reis

Received 3rd October 2023,
Accepted 28th November 2023

DOI: 10.1039/d3ma00797a

rsc.li/materials-advances

Photodynamic therapy (PDT) is a non-invasive procedure used in cancer treatment that requires the interplay of a photosensitizer (PS), a light source, and molecular oxygen. When the cell internalizes the PS, light irradiation will trigger the production of reactive oxygen species (ROS), which induces cancer cell death. Currently, efforts are being made to improve the properties of different PSs, namely their light absorption parameters, pharmacokinetics, and tumor accumulation. Verteporfin (VP) is a protoporphyrin derivative that is under clinical trials for the management of several types of cancer. Despite being approved as a PS in other pathologies, such as age-related macular degeneration, issues related to VP's poor water solubility and tumor accumulation may compromise its efficacy and clinical application. In this work, solid lipid nanoparticles (SLNs) were proposed as suitable nanocarriers of VP. Nanoparticles were produced using a low-cost method and presented high encapsulation efficiency (EE%) and adequate physiochemical properties for efficient delivery into the tumor benefiting from the enhanced permeability and retention (EPR) effect. In addition, SLNs were non-hemolytic and exhibited negligible toxicity under dark conditions in both normal (L929) and cancer (MCF-7) cells. After light irradiation with a LED light source at 690 nm, 6.7 mW $cm^{-2}$ for 5 min, a dose-dependent anti-cancer activity was achieved. These results were corroborated by an enhancement in the production of ROS and a higher degree of apoptosis. Overall, the presented study demonstrated that SLNs are promising candidates to improve the water solubility of VP while maintaining its high therapeutic effect.



## 1. Introduction

Cancer is the major cause of death globally, with 19.3 million new cases and 10 million cancer-related deaths reported in 2020.[1] The limitations and drawbacks of conventional cancer therapies, such as low tumor accumulation and systemic toxicity, highlight the demand for alternative treatment modalities. Photodynamic therapy (PDT) is a minimally invasive therapeutic strategy that requires the combined effects of a photosensitizer (PS), a light source, and oxygen.[2] They induce several photophysical and photochemical reactions, leading to the production of reactive oxygen species (ROS), which will ultimately cause cancer cell death.[2] Different mechanisms elicited by PDT can contribute to tumor destruction, including a direct effect on cancer cells, which may undergo apoptosis or necrosis, damage to the tumor vasculature, and the stimulation of the immune system.[3] The mode and degree of cancer cell death are influenced by the physicochemical properties, concentration, and location of the PS, as well as the oxygen concentration and the intensity and wavelength of the radiation source used.[3,4] Currently, efforts are being made to design PS with enhanced characteristics, in an attempt to make PDT a well-established clinical modality. Ongoing research is focused on developing PS with longer wavelength light absorption, enhanced water solubility, higher tumor accumulation, and improved efficacy.[5,6] Verteporfin (VP), also known as benzoporphyrin derivative monoacid ring A, is a lipophilic protoporphyrin derivative, undergoing clinical trials as a therapeutic strategy for different cancer types.[7] Despite its success in the treatment of diseases such as age-related macular degeneration, VP's clinical application is hindered by its low solubility in aqueous solvents and limited tumor selectivity.[7] In this context, nanotechnology can be a valuable strategy to improve the outcomes of PDT in cancer therapy.[8–12] The use of nanoparticles as drug carriers was found to increase the tumor selectivity, water solubility, stability, and biopharmaceutical performances of different PSs.[8,9,13] Lipid nanoparticles exhibit several characteristics that make them excellent choices as nanocarriers for PDT applications, namely, their suitability to encapsulate hydrophobic drugs, high stability and tolerability, low-cost manufacture, and easy scale-up.

The present work proposes the development of a VP nanocarrier based on solid lipid nanoparticles (SLN) aiming to

*LAQV, REQUIMTE, Departamento de Ciências Químicas, Faculdade de Farmácia, Universidade do Porto, R. Jorge de Viterbo Ferreira 228, 4050-313, Porto, Portugal. E-mail: aagranja@ff.up.pt*

† Electronic supplementary information (ESI) available. See DOI: https://doi.org/10.1039/d3ma00797a

improve its water solubility, enhance tumor retention and reduce non-specific systemic distribution, possibly leading to the reduction of drug doses while achieving a similar therapeutic outcome. To the best of our knowledge, only one study has reported the use of lipid nanoparticles, specifically nanostructured lipid carriers, for the entrapment of VP for PDT of cancer. In the current study, the production of a simpler type of lipid nanoparticles, SLN, was proposed for the delivery of VP and the subsequent PDT was conducted using an economic LED light source, instead of a laser source. Additionally, the mechanism of action of the nanoformulation was thoroughly evaluated. SLNs were produced by a simple, low cost and organic-solvent-free process. A detailed physicochemical characterization and stability study was then conducted followed by the assessment of the hemocompatibility and cytotoxicity in the absence of light of the nanoformulation in a reference cell line (L929) and in the cancer cell line MCF-7, as a proof of concept. After establishing the most suitable light irradiation conditions, the PDT efficacy of the nanosystem was evaluated in MCF-7 cells using a LED light source at 690 nm. The efficiency of the PDT strategy was evaluated by measuring cell viability, quantifying the production of ROS, and determining the induction of apoptosis under light and dark conditions.

## 2. Materials and methods

### 2.1. Materials

Dimethyl sulfoxide (DMSO), Dulbecco's phosphate buffered saline (PBS) 10×, formalin solution neutral buffered 10%, resazurin sodium salt, sodium chloride, Triton X-100, trypan blue, Tween® 80, verteporfin (VP), and 2′,7′-dichlorofluorescein diacetate (DCF-DA) were acquired from Sigma-Aldrich® (St Louis, MO, USA). Cetyl palmitate was provided by Gatefossé (Nanterre, France). Dulbecco's modified Eagle's medium (DMEM), heat inactivated fetal bovine serum (FBS), penicillin–streptomycin and trypsin–EDTA (0.25%) were acquired from Gibco® by Life Technologies™ (UK). Hoechst 33342® was purchased from Invitrogen (Thermo Fisher Scientific, MA, USA). FITC annexin V Apoptosis Detection Kit with 7-AAD was obtained from Biolegend® (California, USA). MCF-7 (passages 77–90) was purchased from ATCC (Middlesex, UK). L929 cells (passages 18–24) were acquired from Cell Lines Service (CLS, Eppelheim, Germany). LS-LED light source with a 690 nm LED slide was purchased from Sarspec (Porto, Portugal).

### 2.2. Production of verteporfin-loaded solid lipid nanoparticles

SLN were produced by the hot ultra-sonication method, as reported earlier.[14] Briefly, the lipid phase comprising 210 mg of cetyl palmitate, 70 mg of Tween® 80, and 5 mg of VP was placed in a water bath at 70 °C. After lipid melting and VP solubilization, pre-heated ultra-pure water (4.4 mL) was added to the lipid melt and subsequently sonicated for 5 min at 70% using a VCX130, Sonics, and a Material Vibra-Cell™ sonicator with a CV-18 probe (USA). The nanoemulsion was then cooled, protected from light with aluminium foil, and stored at 4 °C until further use.

### 2.3. Size, polydispersity index, and ζ potential determination

Particle size, polydispersity index (PdI), and ζ potential were measured by dynamic light scattering and electrophoretic light scattering using a ZetaPALS analyzer (Brookhaven Instruments Corporation, NY, USA). Samples were diluted in ultra-pure water at a ratio of 1 : 400. For each measurement, three runs of 2 min each were completed. Data were obtained by measuring the average of three independent nanoformulations. Particle size was also measured by nanoparticle tracking analysis (NTA, NanoSight NS300, Malvern Instruments, Worcestershire, UK). Samples were diluted in double-deionized water (1 : 10 000) and injected into the system at an infusion rate of 50 at room temperature. Data were obtained based on 5 independent 20 s videos captured with a CMOS camera and analysed using the NTA 3.4 software.

### 2.4. Encapsulation efficiency and loading capacity assessment

The determination of the VP encapsulation efficiency (EE%) and loading capacity (LC%) was performed by UV-vis spectroscopy. Nanoformulations were diluted in ultra-pure water and placed in centrifugal filter units (Amicon®, 50 kDa, Merck Millipore, Darmstadt, Germany) and subsequently centrifuged at 3900 rpm (Multifuge X1R, Thermo Fisher Scientific, USA). The supernatant was then recovered and the absorbance of free VP present in the aqueous phase was determined at 690 nm in a Jasco V-660 spectrophotometer (Jasco Corporation, USA).

The EE% of VP was determined according to the following equation:

$$\mathrm{EE} = \frac{\text{Total amount of VP} - \text{Amount of non-encapsulated VP}}{\text{Total amount of VP}} \quad (1)$$

The LC% of VP was calculated as the ratio between the mass of encapsulated VP and the total mass of lipid used in the nanoformulation, as follows:

$$\mathrm{LC} = \frac{\text{Total amount of VP} - \text{Amount of non-encapsulated VP}}{\text{Total amount of lipid}} \quad (2)$$

### 2.5. Absorption and fluorescence measurements

Absorption spectroscopy measurements were performed using a Jasco V-660 spectrophotometer (Jasco Corporation, USA). The fluorescence spectra were recorded in a Jasco FP-6500 spectrofluorometer (Easton, MD, USA). Measurements were performed in double-deionized water for the nanoformulation and methanol for the free drug.

### 2.6. Stability studies

To study the stability of the nanoformulation, periodic assessments of the particle size, PdI, ζ potential, and EE% were performed over 12 weeks. During the period of the study, nanoparticles were stored at 4 °C. The colloidal stability of the nanoparticles was also evaluated after incubation in several biologically relevant media, namely PBS, PBS with 1% FBS and PBS with 10% FBS at 37 °C over 24 h.

### 2.7. *In vitro* drug release

The release of VP was determined in PBS buffer pH 7.4 (with 5% v/v Tween 80 to guarantee sink conditions) using the dialysis assay. Briefly, free VP and SLN VP were placed in a cellulose dialysis membrane (MWCO 12–14 kDA, Spectrum Labs, CA, USA) and immersed in 70 mL of PBS pre-heated at 37 °C under constant stirring. At specific time intervals, aliquots of 1 mL were withdrawn and an equal volume of PBS was added to the external media. The release content of VP was measured by UV-vis spectroscopy as described previously.

### 2.8. Hemolysis assay

To perform this assay, human blood samples from three distinct donors were provided by Serviço de Hematologia from Centro Hospitalar Universitário do Porto. Before use, blood samples were stored in EDTA-containing tubes. Red blood cells (RBCs) were isolated from the plasma fraction by centrifugation at 955 × *g* for 5 min at 4 °C. After that, RBCs were washed three times with physiological sterile saline solution (0.85% w/v) and diluted in the same solution, to obtain a concentration of 4% (v/v).

The nanoformulations with final concentrations ranging from 2 to 32 μM VP were prepared and incubated with the RBCs at 37 °C for 1 h. A solution of Triton X-100 (1% v/v) and saline solution was chosen as positive and negative controls, respectively. After the incubation period, the amount of released haemoglobin in the supernatant was measured at 540 nm using a microplate reader (Biotek Instruments, Winooski, VT, USA).

The percentage of hemolysis was determined according to the following equation:

$$\text{Hemolysis}\,\% = \frac{\text{Abs (sample)} - \text{Abs (negative control)}}{\text{Abs (positive control)} - \text{Abs (negative control)}} \times 100 \quad (3)$$

### 2.9. Cell viability assay

Cellular viability following incubation with free VP and SLN VP was measured using the resazurin assay. First, cells (L929 and MCF-7) were seeded onto 96-well tissue culture plates (Falcon®, Becton Dickson; England) at a density of $1 \times 10^4$ cells per well and incubated for 24 h at 37 °C, 5% $CO_2$. Free VP and SLN VP were then diluted in DMEM and incubated with the cells. The positive control consisted of cells treated only with DMEM. After 24 h of incubation, a solution of resazurin (10% v/v in DMEM to obtain a working concentration of 0.01 mg $mL^{-1}$) was added to each well. After 2 h of incubation in the dark, the supernatant was transferred to a black-well clear bottom 96-well plate and the fluorescence of the resultant resorufin was measured using a microplate reader (Biotek Instruments, Winooski, VT, USA) ($\lambda_{ex}$ = 560 nm; $\lambda_{em}$ = 590 nm).

For the light-irradiation experiments, MCF-7 cells were seeded in 96 well plates and grown for 24 h. After that, free VP and SLN VP were incubated with the cells for 3 h followed by irradiation with an LS-LED LED light source (an LED slide of 690 nm) coupled to a Vis/NIR optical fiber (50 cm, 600 μm core diameter, Sarspec, Porto, Portugal) at 6.7 mW $cm^{-2}$ for 5 min. The resazurin assay was conducted on the following day, as described before.

### 2.10. Cellular uptake

The internalization of free VP and SLN VP into MCF-7 cells was evaluated using confocal laser scanning microscopy. MCF-7 cells were seeded ($1 \times 10^4$ cells per well) in 8 well-μ-slides (Ibitreat, Ibidi GmbH, Munich, Germany). After 24 h of incubation, free VP and SLN VP (0.125 μM of VP) were added and incubated for 3 h at 37 °C. After rinsing with PBS three times, the cells were fixed with formalin solution for 30 min and stained with Hoechst (8 μM in buffer) for 10 min. Images of cellular uptake were acquired on a Leica Stellaris 8 confocal microscope (Leica Microsystems, Wetzlar, Germany) using a $\lambda_{ex}/\lambda_{em}$ of 405/420–480 nm (Hoechst 33342®) and $\lambda_{ex}/\lambda_{em}$ of 650/680–700 nm (VP). Images were acquired with a resolution of 1024 × 1024 using a 63×/1.4 oil immersion objective. Confocal microscopy assays were carried out at the imaging by Confocal and Fluorescence Lifetime Laboratory at Centro de Materiais da Universidade do Porto (CEMUP), Portugal.

Cellular uptake was also studied by flow cytometry. Briefly, MCF-7 cells were seeded in 24-well plates ($2 \times 10^5$ cells per well) and grown for 24 h. After that, free VP and SLN VP (0.125 μM of VP) were added to the cells and incubated for 30 min, 1 h, 2 h and 3 h. The cells were then detached, centrifuged and resuspended in PBS with 0.004% trypan blue and analyzed in a BD Accuri™ C6 flow cytometer (BD Biosciences, Erembodegem, Belgium) to quantify the fluorescence of VP. Data analysis was conducted using the BD Accuri™ C6 software. The kinetics of cellular uptake was fitted to the Michaelis–Menten equation using Graphpad (GraphPad Prism 6 Software Inc., v.10, CA, USA).

### 2.11. Reactive oxygen species quantification

The production of ROS in MCF-7 cells under dark and light conditions was quantified by flow cytometry using the DCF-DA probe. Briefly, MCF-7 cells were seeded into 96-well plates ($3 \times 10^4$ cells per well) and cultured for 24 h. Subsequently, free VP and SLN VP (at 0.125 μM of VP) were incubated with the cells. For the light irradiation experiments, after 3 h, cells were illuminated with a LS-LED LED light source (LED slide of 690 nm) at 6.7 mW $cm^{-2}$ for 5 min. After that, the medium was removed and DCF-DA (10 μM in PBS) was added to the cells and incubated for 30 min at 37 °C in the dark. The cells were then washed twice with PBS, detached and centrifuged for 5 min at 300 × *g*, and resuspended in PBS. Trypan blue (0.004%) and PI (0.01 mg $mL^{-1}$) were added to quench the signal from extracellular-bound DCF and stain dead cells, respectively. A BD Accuri™ C6 flow cytometer (BD Biosciences, Erembodegem, Belgium) was used to measure the fluorescence of DCF. A minimum of 10 000 events were collected for each sample. Data were examined using the BD Accuri™ C6 software.

### 2.12. Apoptosis assay

The determination of apoptosis elicited after PDT was performed using an FITC annexin V Apoptosis detection kit

according to the manufacturer's instructions. MCF-7 cells were seeded into 96-well plates ($3 \times 10^4$ cells per well) and cultured for 24 h. The cells were then incubated with free VP and SLN VP at an equivalent concentration of 0.250 μM VP. For the light-irradiation experiments, after incubation with the nanoformulations for 3 h, the cells were illuminated with a LS-LED LED light source (LED slide of 690 nm) at 6.7 mW $cm^{-2}$ for 5 min. After 24 h, the cells were detached, and centrifuged for 5 min at 300 × *g*. After washing, the cells were maintained in the annexin V binding buffer, and stained with FITC annexin V and 7-AAD. Apoptosis was measured using flow cytometry, with at least 10 000 events collected for each sample. Data were examined using the BD Accuri™ C6 software (BD Biosciences, Belgium).

### 2.13. Statistical analysis

Statistical analysis was carried out using GraphPad Prism6 software (GraphPad Software Inc., San Diego, CA, USA). Data were analyzed using two-way analysis of variance (ANOVA) with a *p*-value $<0.05$ considered statistically significant. Data are expressed as mean ± SD of at least three independent assays.

## 3. Results

### 3.1. Physicochemical characterization

The main physicochemical characteristics of the produced nanoparticles, namely size, PdI, ζ potential, EE%, and LC% were determined and are presented in Table 1. SLN exhibited a particle size of 193 nm, which is within the optimal size range for blood circulation and subsequent tumor retention, with a lower probability of renal excretion and recognition by the reticuloendothelial system.[15,16] The PdI of 0.16 (<0.2) indicates the presence of a homogeneous nanoparticle population.[17] Additionally, SLN presented a negative ζ potential of −28 and a high drug EE% of 98%, corresponding to an LC% of 2.34. Particle size and size distribution were also evaluated by NTA (Fig. S1, ESI†). A mean particle size of 161 nm was obtained, which is slightly lower than the DLS determinations, due to the higher bias of the latter technique towards the presence of bigger sized-particles.[14] Overall the properties of the SLN suggest that they are suitable nanocarriers of VP and adequate for intravenous administration and passive tumor targeting. The photophysical properties of the nanoformulation and free drug, namely the absorption and fluorescence spectra were also studied (Fig. S2, ESI†). Nanoparticles presented an absorption peak at 690 nm and exhibited a fluorescence emission band in the 680–700 nm region, similar to free VP.

### 3.2. Storage and colloidal stability

To ensure that the main properties of the SLN were not significantly altered during storage at 4 °C, periodic determinations of the particle size, PdI, ζ potential and EE% were performed over time. The data presented in Fig. 1 demonstrate that during 12 weeks, the main properties of the nanoparticles remained unchanged, suggesting the absence of particle aggregation and drug leakage during storage, which indicates that the nanoformulation was stable during this period.

The colloidal stability of the nanoformulations was also assessed by measuring the particle size and size distribution after incubation at 37 °C with PBS, PBS with 1% FBS and PBS with 10% FBS for 1 h and 24 h. The data presented in Fig. S3 (ESI†) show that there were no differences in the particle size and PdI after 24 h, supporting that the nanoparticles were stable in biological-relevant media.

Table 1 Physicochemical characterization of SLN VP: size, PdI, ζ potential, EE%, and LC%. Values expressed as mean ± SD (*n* = 3)

| Size (nm) | PdI | ζ potential (mV) | EE (%) | LC (%) |
|---|---|---|---|---|
| 193 ± 8 | 0.16 ± 0.02 | −28 ± 7 | 98 ± 3 | 2.34 ± 0.06 |

### 3.3. Hemolytic potential

To further evaluate the potential of the produced nanoformulation for intravenous administration, a hemolysis assay was conducted. To do so, different concentrations of free VP and SLN VP were prepared and incubated with human RBCs at 37 °C for 1 h. As shown in Fig. 2, only negligible levels of hemolysis were measured (less than 0.1%) for all the concentrations tested, suggesting that neither free VP nor the SLN VP interacted with the RBC membrane. The presented data highlight that the nanoformulation is non-hemolytic and safe for intravenous administration according to ISO/TR 7406.

### 3.4. Cytocompatibility

An ideal PS should have low dark toxicity, *i.e.*, induce limited cytotoxicity in the absence of light.[2] Following the determination of the absence of RBC toxicity, the cytotoxicity of SLN VP without light irradiation was investigated in two different cell lines and compared to that of the free drug. This was performed in the normal cell line L929, according to the ISO 10993-5 recommendations for biocompatibility assessment (Fig. 3A) and in the breast cancer cell line MCF-7 (Fig. 3B). As shown in Fig. 3A and B, there were no significant changes in cell viability in both normal and cancer cells after incubation with free VP and SLN VP for 24 h. However, a slight reduction in cell viability after treatment with free VP compared to the SLN VP in L929 cells can be observed, suggesting that SLN can protect this normal cell line from some of the intrinsic toxicity of free VP.

Overall these results suggest that the range of concentrations tested is safe and, therefore, suitable to proceed with efficacy PDT studies.

### 3.5. MCF-7 cellular uptake

The uptake of SLN into MCF-7 cells was visualized by confocal microscopy. Cells were incubated with free VP and SLN VP, fixed with formalin solution followed by cell nucleus staining with Hoechst. Incubation with DMEM was used as a control. As observed in Fig. 4, after 3 h a considerable amount of VP can be observed under both conditions, while no fluorescence is found in the cells incubated with only DMEM, suggesting that the fluorescence observed is only attributed to the fluorescence of VP. Moreover, a slightly higher internalization of free VP is observed, when compared to SLN VP. This result is expected,

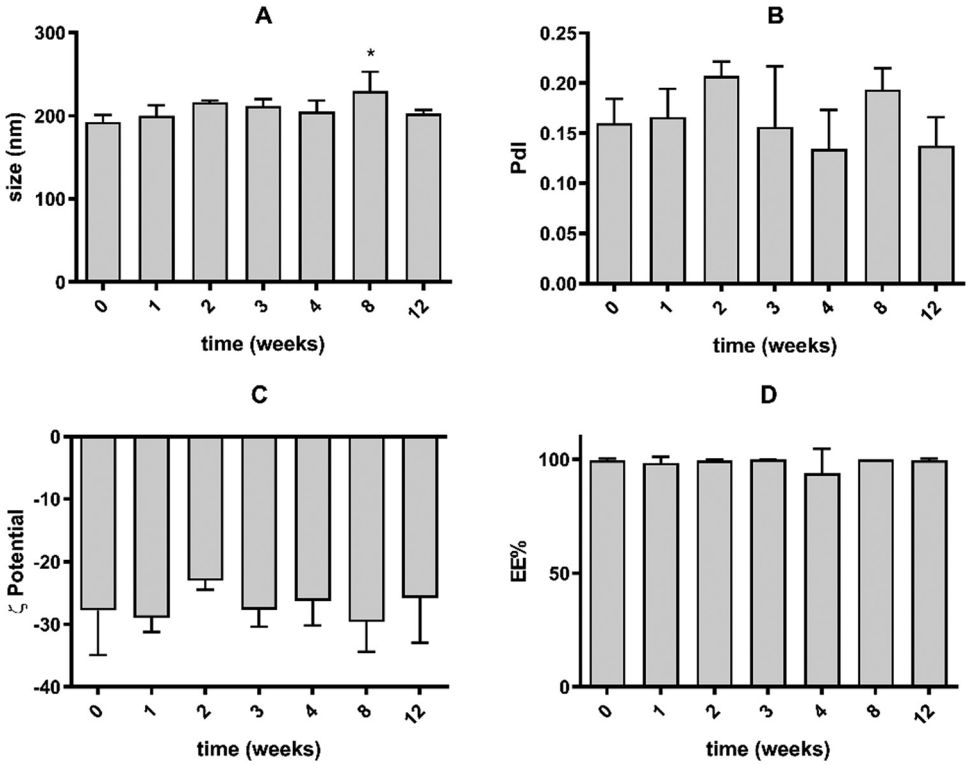


Fig. 1 Storage stability of SLN VP. Periodic determinations of particle size (A), PdI (B), ζ potential (C), and EE% (D) were performed over 12 weeks. Values expressed as mean ± SD ($n$ = 3). Differences between each time-point and time-point 0 were determined using one-way ANOVA followed by Dunnett's test. *$p < 0.05$.

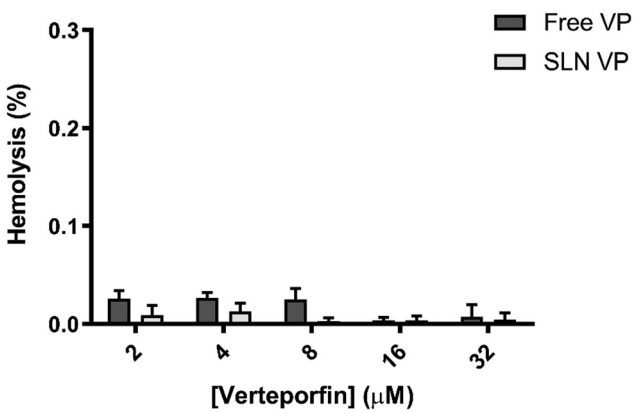


Fig. 2 Hemolysis assay of free and VP-loaded SLN at different concentrations of VP following incubation at 37 °C for 1 h. Data are expressed as mean ± SD (blood collected from 3 independent human donors).

as SLN is internalized by different cellular mechanisms than the free drug and also due to the time-dependent release of VP from the SLN.[18] This latter fact was shown in the drug release assay presented in Fig. S4 (ESI†), where it is possible to observe that VP is released at a lower rate and in a more controlled manner when incorporated into the lipid nanoparticles when compared to the free drug. Nevertheless, the presented data demonstrate that SLN could deliver a significant amount of VP to MCF-7 cells after 3 h of incubation, supporting that this incubation time can be explored in following PDT efficacy studies.

Cellular uptake was also evaluated by flow cytometry. Free VP and SLN VP were incubated with the cells at different time intervals over a 3 h period. The time-dependent cellular uptake and the corresponding Michaelis–Menten parameters are presented in Fig. 5. Both free VP and SLN VP followed Michaelis–Menten kinetics with the internalization of VP detected after 30 min under both conditions. An initial rapid internalization was observed during the first hour, reaching a plateau after 2 h. Free VP was found to be internalized to a greater extent than the nanoparticles, showing a 1.6 higher saturated cellular uptake ($V_{max}$), which is consistent with the previous findings from confocal microscopy and drug release results. Nevertheless, these data clearly demonstrate that the nanoparticles can effectively and rapidly deliver VP to cancer cells, starting as early as 30 min of incubation.

### 3.6. Photodynamic therapeutic effects

**3.6.1. Establishment of the light irradiation parameters.** After determining the optimum VP concentration range and SLN incubation time, the parameters related to the light source, namely, the power density and the irradiation time, were studied to select the ideal conditions for subsequent PDT experiments. In this work, a LED light source with a 690 nm LED slide attached to a Vis/NIR optical fiber was used. Additional information regarding the LED emission spectrum and the setup for the LED irradiation experiments is shown in Fig. S5 (ESI†). The choice of a LED source instead of a laser is related to its lower cost, user-friendliness, portability, and simpler technological requirements.

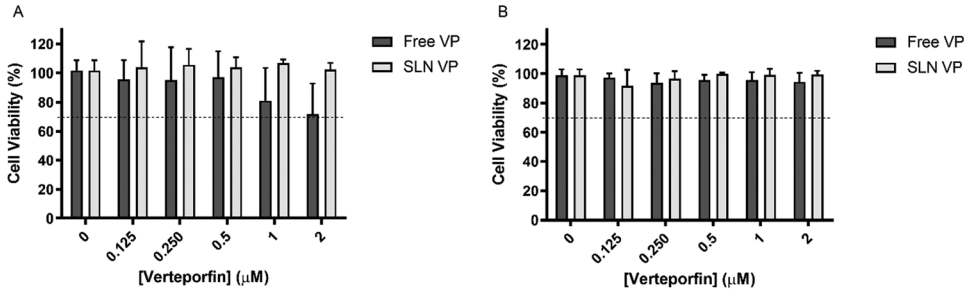


Fig. 3 Cytocompatibility assessment of free VP and SLN VP in fibroblast cell line L929 (A) and cancer cell line MCF-7 (B) after incubation for 24 h. Data are expressed as mean ± SD of three independent assays. Differences between each condition and control group were determined using two-way ANOVA followed by Dunnett's test.

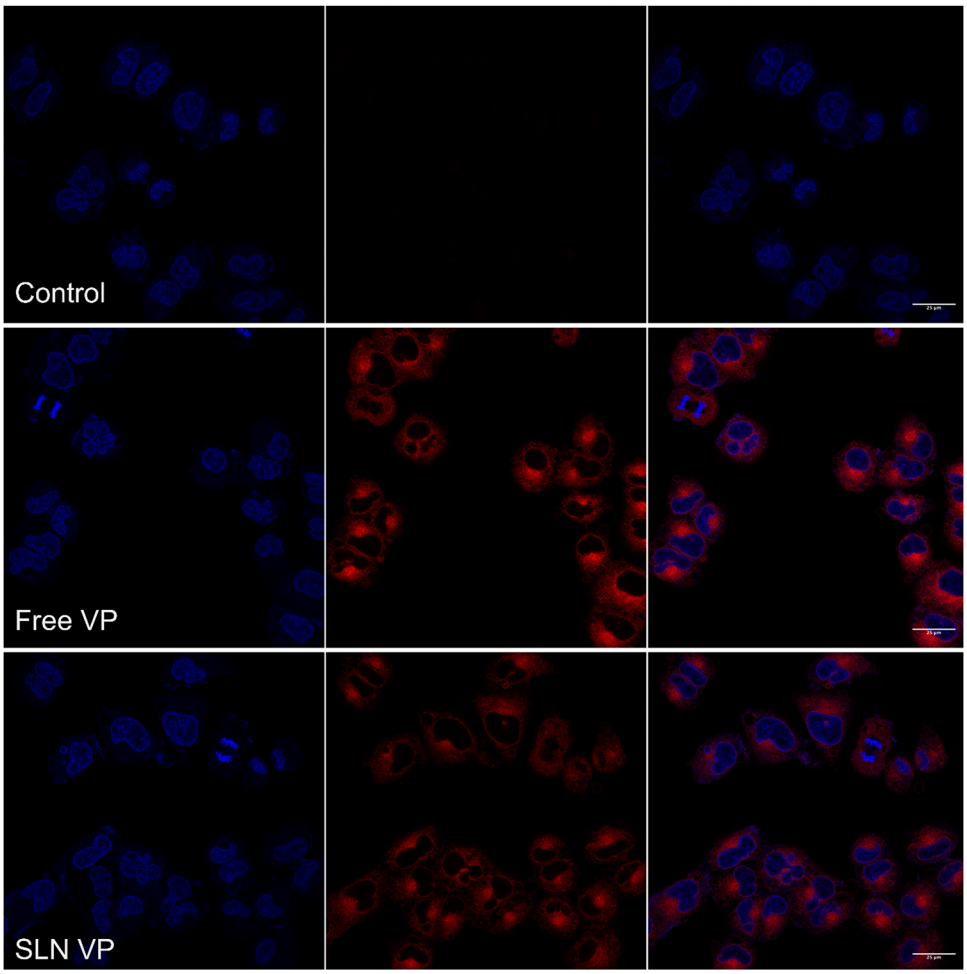


Fig. 4 MCF-7 cellular uptake of free VP and SLN VP after 3 h incubation visualized by confocal microscopy. Blue channel: Hoechst, red channel: VP. The scale bar corresponds to 25 μm.

Nevertheless, compared to diode lasers, LEDs have lower intensity and are unable to produce coherent light, which can impact the wavelength precision.[19] However, given the broad absorption spectra of SLN-VP as demonstrated in Fig. S2A (ESI†), this would not significantly impact the efficiency of the method.

MCF-7 cells were incubated with different concentrations of free VP and, after 3 h, the cells were irradiated at different light power densities (Fig. 6A) and light irradiation times (Fig. 6B). Three different power densities (1.8, 6.7, and 13 mW $cm^{-2}$) and irradiation times (2, 5, and 10 min) were selected. First, the effects of the light *per se* were evaluated by irradiating the cells treated with only DMEM. As shown in Fig. 6A and B, light irradiation by itself did not induce toxicity in MCF-7 cells (with values of cell viability remaining higher than 87%), which demonstrates the safety of the light source used. Nevertheless, it is noteworthy, that in Fig. 6A an increase in the LED power

| | Free VP | SLN VP |
|---|---|---|
| $V_{max}$ | 137659 ± 3205 | 87686 ± 3201 |
| k | 0.42 ± 0.04 | 0.38 ± 0.06 |

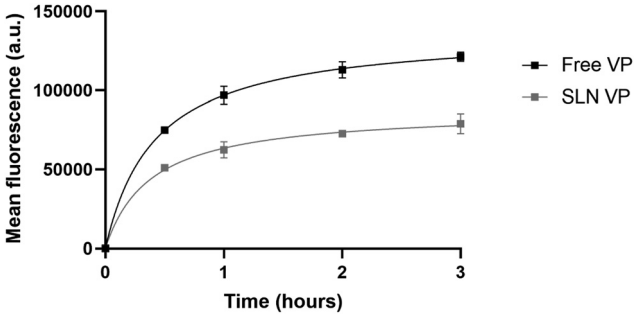


Fig. 5 Michaelis–Menten uptake kinetics of free VP and SLN VP for 3 h in MCF-7 cells measured by flow cytometry. Data are expressed as mean ± SD ($n$ = 3).

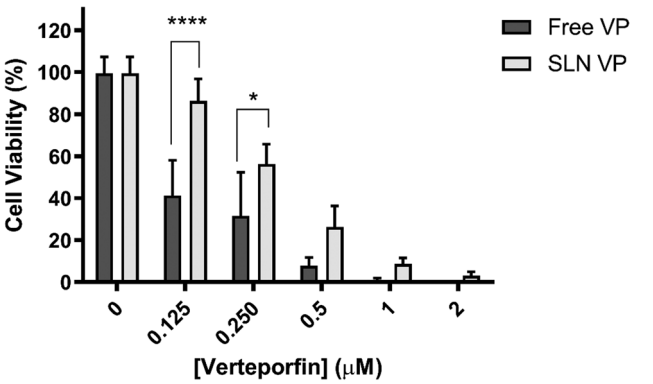


Fig. 7 Photodynamic therapeutic effects of free VP and SLN VP at different VP concentrations in MCF-7 cells. Cells were incubated with free VP and SLN VP for 3 h followed by irradiation with an LED light source at 690 nm for 5 min at 6.7 mW $cm^{-2}$. Cellular viability was measured after 24 h by performing the resazurin assay. Data are expressed as mean ± SD of three independent assays. Differences between free VP and SLN VP were assessed using two-way ANOVA followed by Dunnett's test. *$p$ < 0.05, ****$p$ < 0.0001.

density resulted in a significant decrease in cancer cell viability. A possible explanation for this is that cancer cells can have high susceptibility to visible light exposure, which leads to intracellular metabolic alterations.[20] Furthermore, visible LED irradiation can activate the p53 signaling pathway, thereby suppressing cancer cell proliferation.[20] These facts, however, can be highly dependent on the type of LED source used, wavelength and irradiation parameters chosen.[20]

Concerning the light power density evaluation (Fig. 6A), significant differences in cell viability were found when the power density was increased from 1.8 to 6.7 mW $cm^{-2}$ at 0.5 and 1 μM VP. At the highest power density tested (13 mW $cm^{-2}$), similar outcomes to the ones obtained at 6.7 mW $cm^{-2}$ were observed. Therefore, a power density of 6.7 mW $cm^{-2}$ was selected to proceed with further studies. Regarding the irradiation time study (Fig. 6B), 5 min irradiation induced significantly higher cancer cell death compared to the 2 min irradiation for all the concentrations studied. Light irradiation for 10 min, however, only induced a significant reduction in cell viability compared to 5 min irradiation at the lowest concentration tested (leading to a decrease of 15.2 to 1.5%). Taking this data into consideration and the interest in using irradiation times as short as possible, 5 min irradiation was established for the following PDT efficacy studies. Therefore the following PDT studies were performed using a power density of 6.7 mW $cm^{-2}$ for 5 min, corresponding to a light fluency of 2 J $cm^{-2}$.

**3.6.2. Cellular viability evaluation under light irradiation.** Following the determination of the optimum conditions of irradiation, VP concentration, and incubation time, the photodynamic therapeutic effect of the nanoformulation was assessed in MCF-7 cells and compared to that of the free VP. The cells were incubated with concentrations of VP that were found to be safe under dark conditions (as demonstrated in Section 3.4) and irradiated with an LED light source for 5 min at a power density of 6.7 mW $cm^{-2}$. After 24 h, a resazurin assay was carried out to evaluate the cell viability after PDT, as presented in Fig. 7. As shown in the graph, there was dose-dependent cancer cell

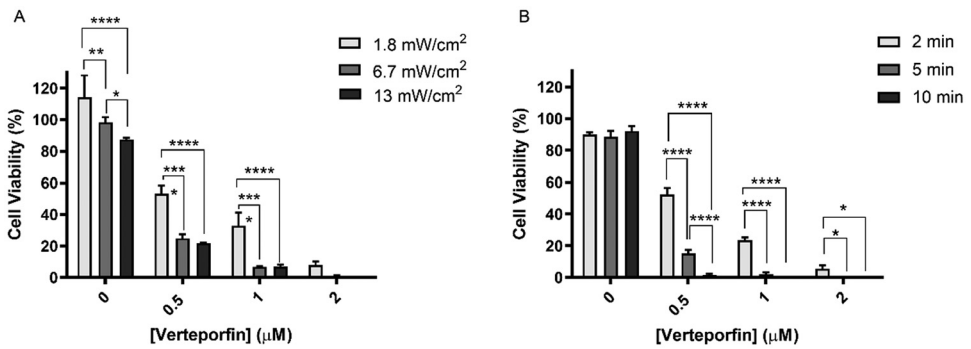


Fig. 6 MCF-7 cell viability evaluation for the selection of the LED light source irradiation parameters. (A) Study of the effect of the power density, with irradiation time set at 5 min. (B) Study of the effect of the irradiation time with power density set at 13 mW $cm^{-2}$. MCF-7 cells were incubated with different concentrations of VP for 3 h, followed by light irradiation at different conditions, as established in the graphs. Cell viability was performed using the resazurin assay 24 h after incubation. Data are expressed as mean ± SD ($n$ = 3). Differences between groups were determined using two-way ANOVA followed by Tukey's test. *$p$ < 0.05, **$p$ < 0.01, ***$p$ < 0.001, ****$p$ < 0.0001.

death, culminating in almost total eradication at the highest concentration tested of 2 μM (with 0 and 2.9% of cell viability after treatment with free VP and SLN VP, respectively). It was also noticeable that free VP elicited a significantly higher cancer cell death at the two lowest concentrations. This could be a consequence of a quicker internalization of the free drug and a time-dependent drug release from the SLN, as suggested by the cellular uptake assays. Nevertheless, at concentrations of VP of 0.5 μM or higher, the effects of the two treatments were similar, as no significant differences were found.

Overall these results support that the mechanism of action of VP as a PS is maintained when incorporated into SLN, being able to induce a high degree of cancer cell death within a range of concentrations without toxicity in the absence of light. Additionally, PDT was conducted using a low-cost light source at a low power density, compared to others found in the literature.[18,21]

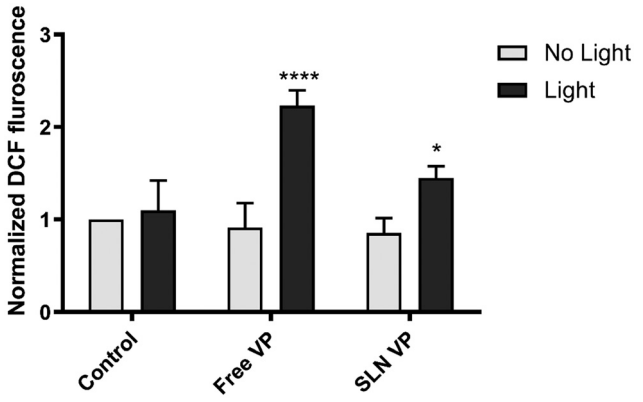


Fig. 8 Determination of ROS production in MCF-7 cells under dark and light conditions after incubation with 0.125 μM free VP and SLN VP for 3 h. For the experiments performed under light conditions, cells were irradiated with an LED light source at 690 nm for 5 min at 6.7 mW $cm^{-2}$. ROS production was quantified by incubating 10 μM probe DCF-DA with the cells for 30 min followed by cell fluorescence quantification of the resultant DCF by flow cytometry. Data are expressed as mean ± SD of three independent assays as normalized mean fluorescence intensity relative to the control group of non-irradiated cells treated with only DMEM. Differences between light and dark conditions were assessed using two-way ANOVA followed by Sidak's test. $p < 0.05$, ****$p < 0.0001$.

**3.6.3. Light-induced reactive oxygen species production.** To study the mechanism of cancer cell death elicited by VP after light irradiation, the production of ROS was quantified under dark and light conditions. To do so, after incubation with the compounds for 3 h and subsequent light irradiation, DCF-DA was incubated with the cells and the fluorescence of the resultant DCF within the cells was quantified by flow cytometry. The data presented in Fig. 8 reveals that in the absence of VP (control treatment), there were no significant differences in cell fluorescence under dark and light conditions, meaning that the light *per se* was unable to induce oxidative stress. This supports, once again, the safety of the light source and irradiation conditions used. The same pattern was found after treatment with both free VP and SLN VP under dark conditions, which elicited negligible levels of ROS production, similar to the control. In contrast, after light irradiation, significantly higher production of ROS was observed after incubation with free VP and SLN VP, with the fluorescence of DCF being 2.4 and 1.7 times higher for free VP and SLN VP, respectively, when compared to their respective values under dark conditions. It is noteworthy that this assay was conducted using the lowest concentration of VP tested, meaning that if higher concentrations were used, a possibly higher production of ROS induced by SLN VP would be measured. Nevertheless, for comparative purposes with the free VP, the lowest concentration was selected to guarantee that the levels of cell death induced would not compromise the flow cytometry assay. Overall, the findings presented in this section are in agreement with the results obtained in Section 3.6.2, suggesting a direct correlation between ROS formation and the reduction of cancer cell viability. In addition, the presented data provide additional evidence that the mechanism of action of VP is maintained when encapsulated into SLN.

**3.6.4. Induction of apoptosis under dark and light conditions.** Since apoptosis is one of the main PDT mechanisms known to elicit cancer cell death,[22,23] the apoptosis triggered by free VP and SLN VP after light irradiation was investigated in MCF-7 cells. To do so, cells were incubated with free drug and nanoparticles, irradiated for 5 min, and, after 24 h, apoptosis was quantified with the FITC annexin V apoptosis kit using flow cytometry. As depicted in Fig. 9A, under dark conditions, 95% of the cells remained viable with only 5% apoptosis detected for the

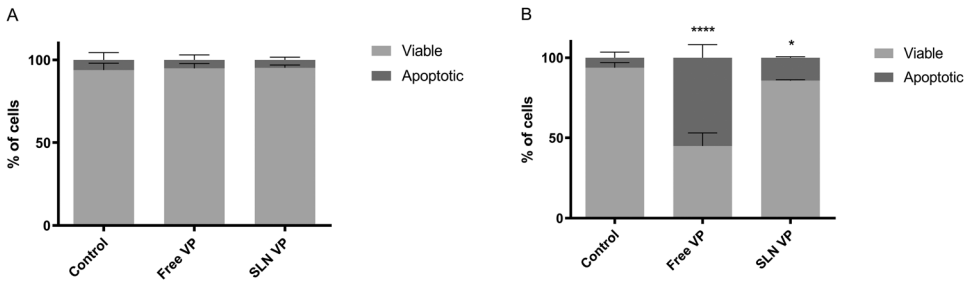


Fig. 9 Apoptosis induction in MCF-7 cells under dark (A) and light (B) conditions: percentage of viable and apoptotic cells. Cells were incubated with 0.250 μM free VP and SLN VP for 3 h and irradiated with an LED light source at 690 nm for 5 min at 6.7 mW $cm^{-2}$. Apoptosis was measured after 24 h using the FITC annexin V apoptosis detection kit with 7-AAD in flow cytometry. Data are expressed as mean ± SD of three independent assays. Differences between conditions were assessed using two-way ANOVA followed by Sidak's test. *$p < 0.05$, ****$p < 0.0001$ compared to the control group.

control and the experimental conditions, supporting the lack of toxicity in the absence of light. Under light irradiation (Fig. 9B), however, there was a significant increase in the percentage of apoptosis for both free VP and SLN VP with 54% and 14% of apoptotic cells detected, respectively, whereas no increase in apoptosis occurred in cells treated with only DMEM. It is important to highlight that, similar to what occurred in the previous section, as free VP was used simultaneously for comparison, to ensure that the levels of cell death induced would not compromise the flow cytometry assay, a low concentration of VP, with possibly lower apoptotic effects induced by SLN VP was chosen.

Overall, these results corroborate the previous data on cell viability and ROS production, demonstrating that SLN could maintain the mechanism of action of VP, namely its apoptotic effects under light irradiation.

## 4. Conclusions

In this study, SLNs were proposed as a simple, low cost and suitable nanocarrier of VP to improve its water solubility and enhance its delivery to cancer cells, while maintaining its high PDT efficiency.

SLNs were produced using a simple, cost effective and organic solvent-free technique, which can more easily enable the large-scale production of this nanoformulation. Nanoparticles presented low PdI ($<0.2$) and adequate size (193 nm) for intravenous injection and passive tumor targeting exploiting the EPR effect. In addition, VP was efficiently incorporated in the lipid matrix of the SLN, as shown by the high values of EE% of 98%. The nanoparticles remained stable for at least 3 months, without significant variations of their main physicochemical characteristics over time. In terms of biocompatibility and safety, the produced SLNs were non-hemolytic, once again supporting its use for intravenous administration, and revealed low cytotoxicity in both normal and tumoral cells. The delivery of VP to MCF-7 cells was found to be effective after 3 h of contact, therefore this incubation time was selected to proceed with the following PDT studies. Those revealed a high cancer cell death effect induced by the nanoformulation, with almost full eradication at the highest concentration tested and comparable effects as the ones obtained for the free drug. This was also corroborated by the enhanced production of ROS and apoptosis induction upon light irradiation, at the lowest concentrations of VP tested (0.125 and 0.250 μM, respectively), suggesting that SLN could maintain the high PDT effect of VP. In the PDT studies, however, free VP induced more immediate anti-cancer effects than the encapsulated VP, possibly due to the occurrence of different cellular uptake mechanisms and a time-dependent VP release from the SLNs. Nevertheless, in all of the studies, the anti-cancer effect of VP was maintained, being able to elicit cancer cell death in a dose-dependent manner, with results comparable to those of free VP. Taking into consideration the benefits of using SLN as VP nanocarriers, such as improved water solubility, reduced off-targeted systemic distribution and toxicity and enhanced accumulation in the tumor region, lower VP doses may be used with similar therapeutic effects. Therefore, the developed nanoformulation can be a promising therapeutic strategy to improve current VP-mediated PDT. Moreover, the PDT reported in this study was conducted using an economic LED light source and low-light doses, which can also be beneficial in future clinical applications.

## Author contributions

Tomás Mendes: investigation and writing – original draft; Andreia Granja: conceptualization, investigation, methodology, and writing – original draft, Salette Reis: conceptualization, supervision, funding acquisition, and writing – review & editing.

## Conflicts of interest

The authors declare no conflict of interests.

## Acknowledgements

This work was financially supported with funding from FCT/MCTES (UIDP/50006/2020) through national funds. The authors also acknowledge the funding from HEALTH-UNORTE I&D&I project (NORTE-01-0145-FEDER-000039) co-financed by the European Regional Development Fund (ERDF), through the NORTE 2020 (Programa Operacional Regional do Norte 2014/2020).

## References

1 H. Sung, J. Ferlay, R. L. Siegel, M. Laversanne, I. Soerjomataram, A. Jemal and F. Bray, *Ca-Cancer J. Clin.*, 2021, **71**, 209–249.
2 S. Kwiatkowski, B. Knap, D. Przystupski, J. Saczko, E. Kędzierska, K. Knap-Czop, J. Kotlińska, O. Michel, K. Kotowski and J. Kulbacka, *Biomed. Pharmacother.*, 2018, **106**, 1098–1107.
3 A. P. Castano, P. Mroz and M. R. Hamblin, *Nat. Rev. Cancer*, 2006, **6**, 535–545.
4 A. P. Castano, T. N. Demidova and M. R. Hamblin, *Photodiagn. Photodyn. Ther.*, 2005, **2**, 1–23.
5 M. Ethirajan, Y. Chen, P. Joshi and R. K. Pandey, *Chem. Soc. Rev.*, 2011, **40**, 340–362.
6 I. S. Mfouo-Tynga, L. D. Dias, N. M. Inada and C. Kurachi, *Photodiagn. Photodyn. Ther.*, 2021, **34**, 102091.
7 A. Greco, G. Garoffolo, E. Chiesa, F. Riva, R. Dorati, T. Modena, B. Conti, M. Pesce and I. Genta, *J. Drug Delivery Sci. Technol.*, 2021, **64**, 102562.
8 K. Deng, C. Li, S. Huang, B. Xing, D. Jin, Q. Zeng, Z. Hou and J. Lin, *Small*, 2017, 13.
9 P. Sanchez-Moreno, J. L. Ortega-Vinuesa, J. M. Peula-Garcia, J. A. Marchal and H. Boulaiz, *Curr. Drug Targets*, 2018, **19**, 339–359.
10 B. Tian, S. Liu, C. Yu, S. Liu, S. Dong, L. Feng, N. Hu and P. Yang, *Adv. Funct. Mater.*, 2023, 2300818.
11 Z. Wang, Q. Sun, B. Liu, Y. Kuang, A. Gulzar, F. He, S. Gai, P. Yang and J. Lin, *Coord. Chem. Rev.*, 2021, **439**, 213945.
12 S. Moghassemi, A. Dadashzadeh, R. B. Azevedo, O. Feron and C. A. Amorim, *J. Controlled Release*, 2021, **339**, 75–90.

13 T. A. Debele, S. Peng and H. C. Tsai, *Int. J. Mol. Sci.*, 2015, **16**, 22094–22136.
14 A. Granja, R. Lima-Sousa, C. G. Alves, D. de Melo-Diogo, M. Pinheiro, C. T. Sousa, I. J. Correia and S. Reis, *Int. J. Pharm.*, 2021, 121044.
15 M. F. Attia, N. Anton, J. Wallyn, Z. Omran and T. F. Vandamme, *J. Pharm. Pharmacol.*, 2019, **71**, 1185–1198.
16 A. Li, S. Wang, Z. Zhang, N. Xu, G. Ling and P. Zhang, *J. Mater. Chem. A*, 2022, **10**, 5191–5202.
17 M. Danaei, M. Dehghankhold, S. Ataei, F. Hasanzadeh Davarani, R. Javanmard, A. Dokhani, S. Khorasani and M. Mozafari, *Pharmaceutics*, 2018, **10**, 57.
18 T. Michy, T. Massias, C. Bernard, L. Vanwonterghem, M. Henry, M. Guidetti, G. Royal, J.-L. Coll, I. Texier and V. Josserand, *Cancers*, 2019, **11**, 1760.
19 S. Lim, H. Jeon, S. Ahn and J. Hahn, *Appl. Sci.*, 2022, **12**, 4176.
20 Y.-J. Kim, J. Song, D.-H. Lee, S. H. Um and S. H. Bhang, *J. Photochem. Photobiol., B*, 2023, **243**, 112714.
21 A. Demiral, N. Verimli, S. İ. Goralı, H. Yılmaz, M. Çulha and S. S. Erdem, *J. Photochem. Photobiol., B*, 2021, **222**, 112261.
22 D. Kessel, *Apoptosis*, 2020, **25**, 611–615.
23 D. R. Mokoena, B. P. George and H. Abrahamse, *Int. J. Mol. Sci.*, 2021, **22**, 10506.